Journal of Theoretical Biology 557 (2023) 111315

Contents lists available at ScienceDirect

Journal of Theoretical Biology

journal homepage: www.elsevier.com/locate/yjtbi

Mechanisms of detachment in fibrillar adhesive systems

Pranav Sudersan, Michael Kappl *

Max Planck Institute for Polymer Research, Ackermannweg 10, 55128 Mainz, Germany

ARTICLE INFO

Keywords:
Fibrillar adhesion
Reversible adhesion
Contact splitting
Beetle
Biomechanics

ABSTRACT

Several creatures can climb on smooth surfaces with the help of hairy adhesive pads on their legs. A rapid change from strong attachment to effortless detachment of the leg is enabled by the asymmetric geometry of the tarsal hairs. In this study, we propose mechanisms by which the hairy pad can be easily detached, even when the hairs possess no asymmetry. Here, we examine the possible function of the tibia-tarsus leg joint and the claws. Based on a spring-based model, we consider three modes of detachment: vertically pulling the pad while maintaining either a (1) fixed or a (2) free joint, or by (3) flexing the pad about the claw. We show that in all cases, the adhesion force can be significantly reduced due to elastic forces when the hairs deform non-uniformly across the array. Our proposed model illustrates the design advantage of such fibrillar adhesive systems, that not only provide strong adhesion, but also allow easy detachment, making them suitable as organs for fast locomotion and reliable hold. The presented approaches can be potentially used to switch the adhesion state in bio-inspired fibrillar adhesives, by incorporating artificial joints and claws into their design, without the need of asymmetric or stimuli-responsive fibrillar structures.

1. Introduction

Over the past few decades, there have been numerous studies to understand how animals, such as geckos and insects, are able to walk on surfaces of any direction while seemingly defying gravity. A microscopic observation reveals that, in many cases, animals have a dense array of fibrillar structures at the end of their legs (Hooke, 1665; Stork, 1980). These *hairy* adhesive pads help the animal to stay attached to any surface or detach easily at will for countless cycles, a property that is referred to as *reversible adhesion*. Previous attempts to theoretically explain adhesion in hairy pads (Labonte and Federle, 2015; O'Rorke et al., 2016; Popov et al., 2016) has followed two fundamental approaches: either by energy balance, or by force balance.

In the energy balance approach, adhesion is usually characterized by *work of adhesion* (W_{adh}), which is the energy required to separate a pad from the surface. During detachment, the elastic energy stored in the hair is dissipated, that increases W_{adh} and thus adhesion is enhanced (Persson, 2003; Jagota and Stephen, 2002). Detachment of an individual hair can be explained based on Kendall's peeling theory (Kendall, 1975; Endlein et al., 2013), which predicts low adhesion at high peeling angles.

In the force balance approach, adhesion is characterized by *pull-off force*, F_p (or stress, σ_p), which is the minimum force necessary to separate two surfaces from contact. Based on a *cohesive zone model*, Hui et al. (2004) have identified two regimes of single hair detachment: (1) a *flaw sensitive* regime, where, for large hair radius, contact failure occurs due to crack propagation, initiated by a stress singularity at the edge of the hair, leading to low σ_p; (2) a *flaw insensitive* regime, where, for small hair radius, the contact interface fails simultaneously, leading to high σ_p. Likewise, Tian et al. (2006) have shown that the spatula-shaped hair tips in a gecko's toe allows it to change adhesion by three orders of magnitude by laterally sliding and controlling the pulling angle to disorient the hairs. The detailed mechanics of the spatula-shaped hair design for controlling adhesion have been extensively studied by theoretical modelling (Pantano et al., 2011; Sauer and Holl, 2013; Wu et al., 2015; Kligerman et al., 2020; Grill et al., 2021; Gouravaraju et al., 2021), artificial mimics (del Campo et al., 2007; Murphy et al., 2007; Mengüç et al., 2012; Chary et al., 2013; Kim and Varenberg, 2017) as well as in several biological systems (Autumn et al., 2000; Langer et al., 2004; Varenberg et al., 2010). Federle (2006) has further argued that the curved shape of the hair helps the pad to stay attached when pulled proximally and easily detached by elastic recoil when pushed distally.

The theory presented so far suggests that a low detachment force of a fibrillar adhesive pad can be achieved either by increasing the stress concentration by peeling the pad at high angles, or by laterally shearing the pad before pull-off, which requires the hairs to have an asymmetric geometry or curvature. However, some insects like male dock beetles predominantly possess mushroom-shaped hairs with flat discoid terminals on their pads (Bullock and Federle, 2009), that are relatively less

* Corresponding author.
E-mail address: kappl@mpip-mainz.mpg.de (M. Kappl).

https://doi.org/10.1016/j.jtbi.2022.111315
Received 6 May 2022; Received in revised form 24 September 2022; Accepted 10 October 2022
Available online 2 November 2022

asymmetric compared to the spatula-shaped hairs. These mushroom-shaped hairs have in fact been shown to possess superior adhesion compared to the spatula-shaped hairs (Carbone et al., 2011; del Campo et al., 2007) and are generally resistant to detachment via lateral shear (Heepe et al., 2014). Yet, how does the beetles possessing such mushroom-shaped hairs still easily detach their legs during locomotion? Besides, from an application perspective, introducing asymmetry into the pillar geometry to construct spatula-shaped artificial biomimetic adhesives for easy detachment is challenging due to current limitations in fabrication techniques and difficulty in scaling-up (del Campo et al., 2007). Alternate strategies are thus desired to switch the adhesion state of symmetric pillar arrays in a reversible manner. This can be achieved, for example, by buckling the pillars under compressive load leading to their contact loss (Paretkar et al., 2013) or by using special materials reacting to external stimuli such as magnetic field (Drotlef et al., 2014), UV light (Kizilkan et al., 2017) or temperature (Cui et al., 2012).

Employing the force-balance approach, in this work we theoretically model the possible mechanisms by which adhesive pads with axially-symmetric hairs can be easily detached, without the need of any spatula-like asymmetry. Here, we focus our analysis on normal adhesion force necessary to separate the pad from a flat surface under a purely mechanical action. We found that the maximum force necessary to detach the leg can be significantly reduced by strategically controlling the tilt, joints and claws of the adhesive system. We hope our work to provide new approaches to control the adhesion force of an artificial micro-pillar adhesive, that has applications in bio-inspired climbing robots, pick-and-place operations and reusable adhesives.

2. Model

Similar to previous approaches (Schargott et al., 2006; Bacca et al., 2016), the fibrillar adhesive pad is assumed to be a one-dimensional array of N_t hairs, each behaving like a spring with spring constant, k_h, and natural length, $l_{h,0}$ (Fig. 1). The array backing is assumed to be stiff. The pad is attached to a linearly deformable leg (tibia), assumed to be another spring with spring constant, k_l, and natural length, $l_{l,0}$. The leg is hinged to the array at a distance, s, from the right end of the array. The hinge, analogous to the tibia-tarsus leg joint of an insect, is at a vertical distance, d_s, from the surface. The hairs are spaced apart by a width, w, and the array is of length, $L = (N_t - 1)\, w$. The pad is oriented at an instantaneous angle, θ, while making contact with a flat smooth surface. Each hair can attain a maximum length, $l_{h,p}$, before pull-off, such that its pull-off force, $f_p = k_h (l_{h,p} - l_{h,0})$. F_{net} is the net normal force on the pad and M_{net} is the net moment about the hinge, at a particular instant during the detachment process. We focus only on vertical detachment modes and thus lateral friction forces between the hairs and surface are not considered for our analysis.

Suppose at a particular instant, there are n hairs in contact with the surface. The net force on the whole pad will be,

$$F_{net} = \sum_{i=1}^{n} k_h \left(l_{h,i} - l_{h,0}\right)$$

Simplifying, we get (see Appendix B for derivation):

$$F_{net} = n k_h \left[d_s - l_{h,0} - \Psi \sin\theta\right] \tag{1}$$

where, $\Psi = s - \frac{n-1}{2} w$. For a particular value of n, Eq. (1) is valid until a certain distance, $d_{s,max}$, above which the left most hair will detach. Just before detachment, this hair will be at its maximum length, $l_{h,p}$. From simple geometry we can thus find:

$$d_{s,max} = l_{h,0} + \frac{f_p}{k_h} + [s - (n-1)\, w] \sin\theta \tag{2}$$

Eq. (1) will be valid for $d_s \le d_{s,max}$.

The maximum possible adhesion of the array would be the case when all hairs detach simultaneously ($\theta = 0°$):

$$F_{max} = N_t f_p \tag{3}$$

The net moment, M_{net}, about the joint can be similarly derived (see Appendix B):

$$M_{net} = n k_h \cos\theta \left[\left(d_s - l_{h,0}\right)\Psi - \left\{\Psi^2 + \frac{n^2 - 1}{12} w^2\right\} \sin\theta\right] \tag{4}$$

Let us now consider the scenario where even the leg above the joint can undergo elastic stretching together with the hairs. When a hair detaches from the surface, the leg undergoes an elastic recoil due to the stored elastic energy. Suppose the leg relaxes upward by a recoil length, Δl, at the point of the joint. For n hairs in contact, when a hair detaches, the array's tilt angle will change from initial θ_b to θ_a as a result of joint rotation. The ith hair of the array thus deforms by Δl_i, which by geometry, is derived as:

$$\Delta l_i = \Delta l + i w \left(\tan\theta_a - \tan\theta_b\right) \tag{5}$$

The force balance before and after a hair detaches is thus given respectively by:

$$\sum_{i=1}^{n} k_h \left(l_{h,i} - l_{h,0}\right) = k_l \left(l_l - l_{l,0}\right)$$

$$\sum_{i=1}^{n-1} k_h \left(l_{h,i} + \Delta l_i - l_{h,0}\right) = k_l \left(l_l - \Delta l - l_{l,0}\right)$$

Solving the above two equations with Eq. (5) for Δl, we get:

$$\Delta l = \frac{f_p - k_h w (n/2)(n-1)\left(\tan\theta_a - \tan\theta_b\right)}{k_h (n-1) + k_l} \tag{6}$$

Thus, d_s shifts by Δl in Eqs. (1) and (4) at each event of hair detachment (i.e. when $d_s = d_{s,max}$).

We express the forces and distances in non-dimensional forms, as below:

$$\hat{f}_p = \frac{f_p}{k_h w}, \quad \hat{F}_{net} = \frac{F_{net}}{k_h w}, \quad \hat{d}_s = \frac{d_s - l_{h,0}}{w}, \quad \hat{s} = \frac{s}{L}$$

Here, $\hat{f}_p$ is a parameter which encapsulates the hair's adhesion force, stiffness and array density. Unless specified, positive force values represent attraction by convention. Python scripts were written to solve the above equations under specific detachment conditions (available in the public repository https://github.com/PranavSudersan/paper-effect_of_tilt/blob/main/codes/Fibrillar%20adhesion%20-%20Effect%20of%20tilt.ipynb)

3. Detachment mechanisms

We consider three tentative scenarios to detach the adhesive pad from a surface: (1) *Fixed pull*, where the pad is pulled vertically up while keeping a fixed joint; (2) *Free pull,* where the pad is pulled vertically up while keeping the joint free to allow rotation of the array; (3) *Flex*, where the pad is hinged to an external point (claw-hinge), and detached in a rotary fashion, emulating the claw function in insects. To investigate each case in detail, let us assume a pad to be a one-dimensional analogue of a dock beetle's adhesive pad (Bullock and Federle, 2009, 2011) with $N_t = 25$ hairs and $\hat{f}_p = 0.1$ (see discussion on *detachment pathways* for details) attached to a stiff leg (or tibia) with $k_l \to \infty$. The situation of a soft leg with $k_l/k_h = 10$ is also considered for the first two cases involving vertical detachment.

3.1. Fixed pull

The fibrillar adhesive pad can be detached by pulling it vertically upwards while maintaining a constant tilt angle, θ, with the surface. This can be achieved if the joint is kept fixed. Eqs. (1)–(3) can be used to get the resulting force–distance curves for such a scenario. To summarize the numerical procedure in brief, we start with an initial $n = 25$ hairs. F_{net} is then calculated for increasing d_s, until $d_s = d_{s,max}$, upon which n value is decremented by 1. The above process is repeated for increasing d_s until $n = 0$, indicating complete detachment. For the

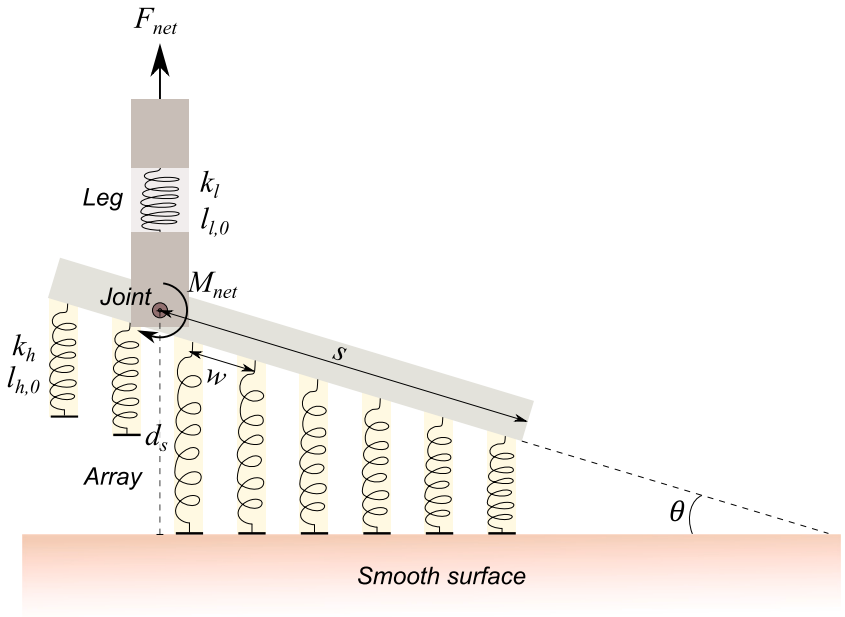

Fig. 1. Spring contact model of a fibrillar adhesive pad. The pad consists of an array of N_t hairs connected to a deformable leg at the joint. At a particular distance, d_s, n number of hairs are in contact and the array is oriented at a tilt angle, θ, with the surface.

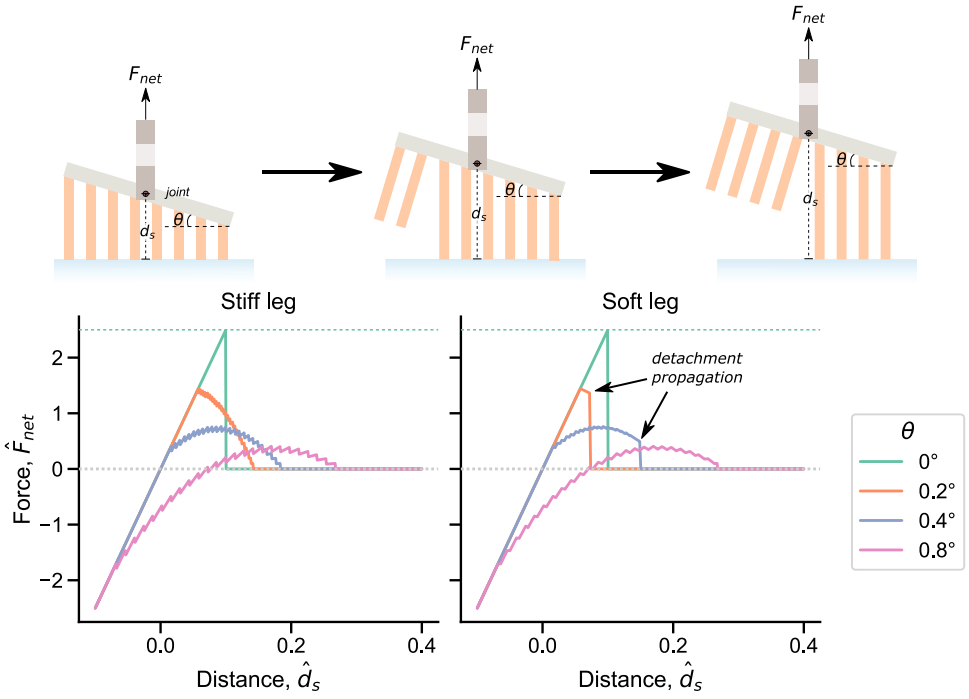

Fig. 2. Detachment by *Fixed Pull*. Force–distance curves for a fibrillar adhesive pad, pulled vertically upwards with a fixed joint. The tilt angle, θ, of the array is kept fixed during detachment. The leg (tibia) is either stiff ($k_l \to \infty$) or soft ($k_l/k_h = 10$). Positive force values represent attraction between the array and the surface. The green dashed line represents the maximum possible adhesion for the pad. All values are normalized to dimensionless forms, as described in text.

case of the soft leg, on each instance when n is decremented, d_s is increased by an additional Δl value (Eq. (6)) in order to account for the recoil effect of the leg.

Increasing the tilt of the pad decreases its maximum force or adhesion (Fig. 2). Tilting the pad causes an inhomogeneous deformation of hairs, where, on one end they are stretched, while, on the other end they are compressed. The balance of the respective attractive and repulsive elastic forces of the hairs ultimately results in a decrease in the net force. The tilted orientation also causes the individual hairs to detach distinctly rather than simultaneously, further reducing the maximum adhesion of the array. We term this effect of loss in adhesion due to a non-uniform hair deformation across the array as *elastic weakening*. When there is no tilt ($\theta = 0°$), all the hairs undergo identical deformation and ultimately detach simultaneously after a distance, $\hat{d}_s = 0.1$. Here, no *elastic weakening* occurs and the pad shows the maximum possible adhesion.

For the case of a stiff leg (tibia), we see that at small distances, all hairs of the pad are in contact with the surface, resulting in a linear force response. On further pulling, the hairs will start to detach sequentially from left to right, indicated by a characteristic saw-tooth

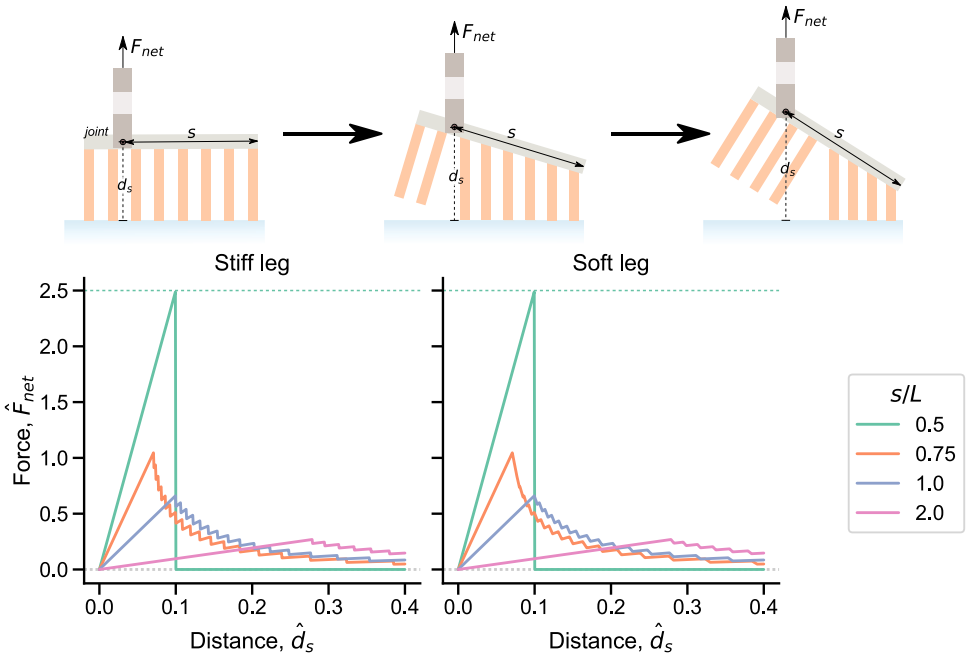

Fig. 3. Detachment by *Free Pull*. Force–distance curves for a fibrillar adhesive pad, pulled vertically upwards with a free joint. s is the distance between the joint and the right end of the array and L is the array length. The free joint allows further tilting of the array during the vertical pull. The leg (tibia) is either stiff ($k_l \to \infty$) or soft ($k_l/k_h = 10$). Positive force values represent attraction. The green dashed line represents the maximum possible adhesion for the pad. All values are normalized to dimensionless forms, as described in text.

jitter in the force curves. The pad with a higher tilt angle initiates hair detachment first, in comparison to a pad with a lower tilt.

For the case of a soft leg (tibia), we observe a similar effect of tilt angle on the force curves as before. The maximum adhesion force at a particular tilt is the same as that for the stiff leg. The saw-tooth jitter are however minimized due to the leg's deformation, leading to a dampened force response. Interestingly, the force abruptly drops to zero for the angles 0.2° and 0.4°. This is an effect of the elastic recoil of the leg while each hair loses contact during the detachment process (Eq. (6)). The length difference between the detached hair just before it breaks contact and its adjacent hair is $w \sin\theta$. If the leg's recoil length, $\Delta l > w \sin\theta$, the adjacent hair will be stretched more than its maximum length ($l_{h,p}$), and thus will also detach, leading to further recoil of the leg. Eq. (6) shows that Δl increases with every subsequent loss of hair contact if θ is kept constant (i.e. $\theta_b = \theta_a$). This implies that, once initiated, the leg's recoil will always be large enough to detach every remaining hair, resulting in a spontaneous propagation of the detachment front until the pad completely breaks contact with the surface. This is consistent with a recent report of catastrophic failure, due to a similar recoil effect of the measurement system, seen in micro-fibrillar adhesives with a narrow variance of individual fibril adhesive strengths (Hensel et al., 2021).

3.2. Free pull

Similar to the previous case, we once again consider the situation where the adhesive pad is pulled vertically upwards for detachment. However now, the joint is assumed to be freely movable. In this case, the array will reorient itself to maintain a zero net moment about the joint during the entire detachment process. At any given instant, the tilt angle, θ, can be found by setting M_{net} to zero in Eq. (4) to get:

$$\theta\left(\hat{d}_s, n\right) = \arcsin\left[\frac{\left(\hat{s} - \frac{n-1}{2}\right)\hat{d}_s}{\left(\hat{s} - \frac{n-1}{2}\right)^2 + \frac{n^2-1}{12}}\right] \tag{7}$$

Using the above relation together with Eqs. (1)–(3), we can find force–distance curves during a free vertical pull of the adhesive pad. A similar numerical procedure as *fixed pull* is followed here. Since the position of the joint will influence the net moment, we use the ratio, s/L, to study its effect on the detachment forces.

Maximum adhesion is seen when the joint is positioned at the centre of the array, i.e. $s/L = 0.5$ (Fig. 3). Here, the net moment due to the hairs is balanced by symmetry and the array remains parallel to the substrate until all hairs detach simultaneously at $\hat{d}_s = 0.1$. Shifting the position of the joint further away from the array centre leads to lower forces or adhesion. The resulting moment imbalance will tilt the array, which reduces the net force due to the *elastic weakening* effect, as described in the previous section. Higher s/L increases the net moment to be balanced, leading to a higher tilt of the array and thus lower net force.

The force curves look qualitatively different compared to the previous case of *fixed pull*. A sharp maxima is seen, coinciding with the point when the first hair detaches. Beyond this, the force starts to decrease sharply and once again shows the characteristic saw-tooth jitter as the subsequent hairs detach in sequence. Nearly identical trend is seen for both a stiff and a soft leg (tibia). The elastic recoil of the leg does slightly reduce the amplitude of the jitter for the soft leg case. However, no abrupt drop in the force is seen like before. As the hairs detach, the array gets tilted more and more (i.e. $\theta_b < \theta_a$), making it less likely for the recoil length, Δl, to exceed $w \sin\theta_a$ and detach the next adjacent hair. Thus here, we do not see any propagation of the detachment front when the leg is soft.

3.3. Flex

Instead of a vertical pull, the adhesive pad can also be detached by rotating it about the claw-hinge, located outside the array. Such a mode of detachment will be driven by a moment applied by the leg (tibia) to rotate the pad around the claw-hinge until all the hairs lose contact. Let s_h be the distance between the claw-hinge and the right end of the array; s_l be the distance between the joint and the right end of the array. The joint is assumed to be fixed here. To illustrate the mechanism, let us fix $s_l/L = 1$ (here, $L = 24w$) and $s_h/w = 10$ and vary the vertical claw-hinge distance, d_s. At any particular instant, the

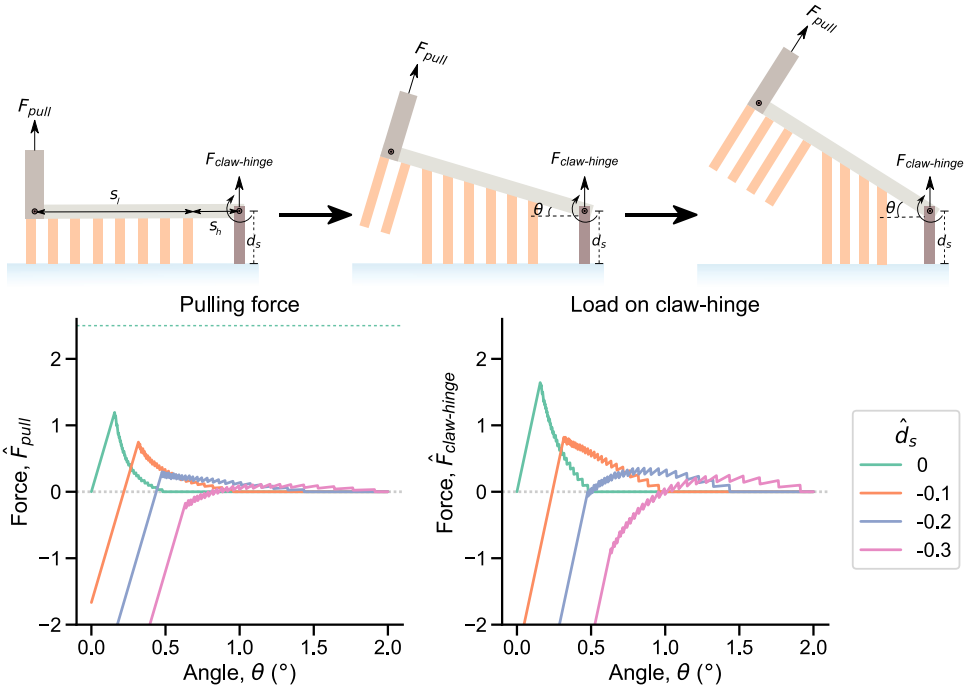

Fig. 4. Detachment by *Flex*. Force curves for a fibrillar adhesive pad detached by flexing it about the claw. $\hat{F}_{pull} = \frac{F_{pull}}{k_h w}$ is the normalized pulling force necessary to apply the moment about the claw-hinge for detachment, $\hat{F}_{hinge} = \frac{F_{hinge}}{k_h w}$ is the normalized reaction force on the claw-hinge, $\hat{d}_s = \frac{d_s - l_{h,0}}{w}$ is the normalized vertical distance of the claw-hinge from the surface. Here, $s_l/L = 1$ and $s_h/w = 10$. The green dashed line represents the maximum possible adhesion for the pad.

pulling force applied by the leg, $F_{pull} = M_{net}/(s_l + s_h)$, where M_{net} is obtained by setting $s = -s_h$ in Eq. (4). Eq. (1) will give us the reaction force acting on the claw-hinge, $F_{claw-hinge}$.

Decreasing the vertical claw-hinge distance reduces the pulling force necessary to undergo detachment by flexing (Fig. 4). One can imagine that initially, when the array is parallel to the surface, a lower value of d_s means the hairs are in a more compressed state. When the pad is subsequently rotated around the claw-hinge, the tilted array will once again lead to an *elastic weakening* effect due to the inhomogeneous deformation of hairs. This results in a decrease in the net moment and thus lower F_{pull} for smaller values of d_s. F_{pull} can be further reduced of course by increasing the lever arm $(s_l + s_h)$.

Detachment by flexing requires that the claw remains fixed and stable during the process. We see that generally, the normal load, acting on the hinge, $F_{claw-hinge}$, follows a similar trend as F_{pull} (Fig. 4). For low values of d_s, $F_{claw-hinge}$ goes to negative values, implying that the claw should stick well with the surface, perhaps by mechanical interlocking, to resist this negative load. As the detachment progresses however, the array starts to exert a positive load on the claw.

4. Discussion

In order to characterize how a particular detachment mechanism influences the adhesion of the pad, we introduce a parameter, *reduction factor*, defined as:

$$r = \frac{N_t f_p}{F_{adh}} \tag{8}$$

Here, F_{adh} is the adhesion force required to detach the pad from the surface following a given mechanism and $N_t f_p$ is the maximum possible adhesion of the pad (Eq. (3)). Reduction factor, r, represents the extent to which the adhesion can be reduced by choosing the mode of detachment. A large value of r implies that adhesion can be reduced by a greater factor, and this mode is more suitable to easily detach.

Effect of $\hat{f}_p$*:*. The dimensionless parameter, $\hat{f}_p = \frac{f_p}{k_h w}$, governs the strength and compliance of the array, where, high values represent a dense array of strongly adhering soft hairs. Let us consider the case of an adhesive pad with $N_t = 25$ hairs and look at how $\hat{f}_p$ influences the reduction factor under each mode of detachment (Fig. 5).

When detachment follows the *fixed pull* method (Fig. 5), for a constant $\hat{f}_p$, the reduction factor increases with increasing tilt angle, θ, and then decreases, showing a maximum r of 25 at an intermediate θ. Higher values of $\hat{f}_p$ shifts this maximum point to higher values of θ. This trend relates to the *elastic weakening* effect discussed before. Smaller values of θ bring a proportion of hairs under compression, reducing the adhesion and thus increasing r. On further tilting the array, eventually the proportion of stretched hairs will overcome the ones under compression, which ultimately reduces r at high θ. When the individual hairs show strong adhesion (i.e. for high $\hat{f}_p$), a greater tilt is necessary to bring the net adhesion of the array down.

For the case of detachment via *free pull*, $\hat{f}_p$ has no influence on the reduction factor. On the other hand, shifting the position of the joint further away from the array (i.e. high s/L) results in large values of r. In this scenario, the higher moment exerted by the array leads to a higher tilt, and thus increases the reduction factor via *elastic weakening*, saturating to the maximum value of 25.

For detachment by *flexing*, the reduction factor increases for higher initial compression of hairs (low $\hat{d}_s$). The pad notably shows a much higher reduction factor at low values of $\hat{f}_p$ and $\hat{d}_s$, with values as high as 100. Since this mode of detachment is driven by moment, the pulling force necessary to provide the moment can be decreased without any limit simply by having a long lever arm ($\hat{s}_l$), i.e., with the joint positioned farther away from the array. In contrast, for the previous cases of *free pull* and *fixed pull*, the reduction factor is capped to the maximum number of hairs in the array ($N_t = 25$). Here, *elastic weakening* can only reduce the array's adhesion force from N_t hairs down to a single hair at most.

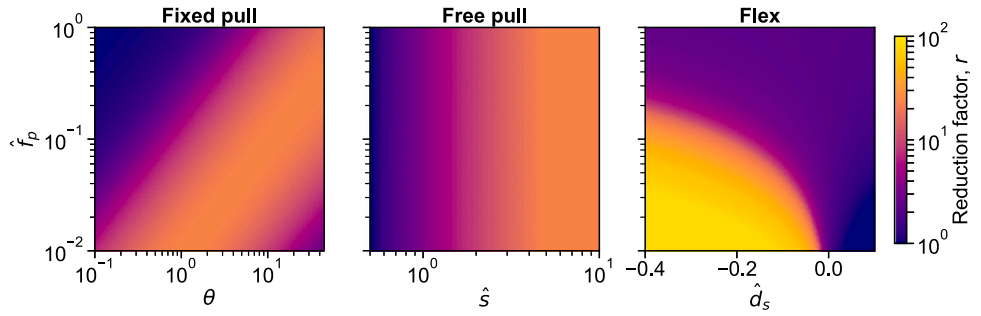

Fig. 5. Effect of $\hat{f}_p$ on reduction factor. Colour plots showing the effect of the dimensionless parameter, $\hat{f}_p$, on the reduction factor for each mode of detachment. Here, we fix the number of hairs, $N_t = 25$. The dimensionless parameters $\hat{d}_s = \frac{d_s - l_{h,0}}{w}$ and $\hat{s} = \frac{s}{L}$, as described in text.

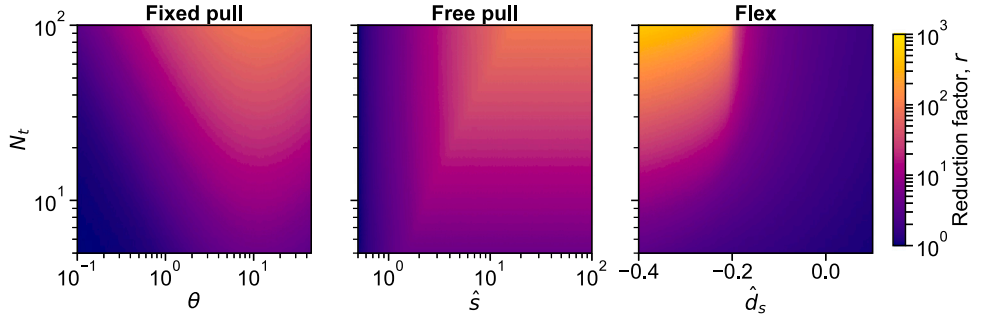

Fig. 6. Effect of N_t on reduction factor. Colour plots showing the effect of the number of hairs, N_t, on the reduction factor for each mode of detachment. Here, we fix the dimensionless parameter, $\hat{f}_p = 0.1$. The dimensionless parameters $\hat{d}_s = \frac{d_s - l_{h,0}}{w}$ and $\hat{s} = \frac{s}{L}$, as described in text.

Effect of N_t:. Let us now fix $\hat{f}_p = 0.1$ and investigate the influence of the number of hairs, N_t, on the reduction factor (Fig. 6). The colour plots show that high N_t increases r irrespective of the mode of detachment. Under a tilted state, more hairs are compressed when N_t is high, which reduces the net adhesion. This highlights another advantage of having a split contact design found in many biological systems. A design comprising of a large number of hairs not only enhances the adhesion due to scaling effects (Kamperman et al., 2010), but could also offer a better control over adhesion, making it quite suitable for reversible attachment and detachment during locomotion. The specific trends of reduction factor for each mode of detachment can be understood by similar arguments of *elastic weakening*, as discussed in the previous section.

Figs. 5 and 6 can be combined into a single set of colour plots by defining a new dimensionless parameter, $\chi = \hat{f}_p N_t = \frac{f_p N_t}{k_h w}$ (see Appendix A). Overall, we see that *flex* mode of detachment shows the highest reduction factor among the three modes, with the optimal value of $\chi \sim 1$.

Detachment pathways:. Based on the three modes of detachment discussed in the previous sections, one can think of several strategies to detach fibrillar adhesive pads from the surface. To illustrate this, let us consider the adhesive system of a dock beetle. The beetle is known to have 3 sets of hairy tarsal adhesive pads in each of their legs, each possessing hairs of different geometries. To keep our analysis simple, we will assume each leg to have only two adhesive pads, with identical hairs of mushroom-shaped geometry. The distal and proximal pads possess roughly 500 and 1000 hairs, respectively (Bullock and Federle, 2009). Assuming the pads to be rectangular arrays of 20 × 25 and 40 × 25 hairs, we can model this as a one-dimensional system of 20 and 40 *effective hairs*, respectively, by combining the hairs along the width. Based on reported measurements (Bullock and Federle, 2011), the beetle's *effective hair* is thus considered to have an effective pull-off force, $f_p = 0.5 \times 25 = 12.5$ μN and effective spring constant, $k_h = 0.5 \times 25 = 12.5$ N m^{-1}. The beetle's hairs are approximately $l_{h,0} = 40$ μm long, spaced $w = 10$ μm apart. At end of the tarsal segments, there is a claw, around 200 μm long, and the leg (tibia) is connected roughly at the end of the proximal tarsal pad. This will put $\hat{s}_h = 20$ and $s_l/L = 1$, measured relative to the right end of the distal pad. The beetle's leg is assumed to possess two joints which could serve as a hinge for rotation during detachment (H_1 and H_2 in Fig. 7 inset). The claw can be used as an external hinge (H_3) by flexing the tarsal pad around it.

Based on the above assumptions, we can come up with force–distance curves to detach the beetle's leg via various pathways (Fig. 7). First, let us assume the joint H_2 to be fixed, such that both the distal and proximal pads can be combined to behave like a single long pad with $N_t = 60$ hairs. Path 1 shows the case where the pad shows maximum possible adhesion. Here, the combined pad is vertically pulled upwards while keeping the array perfectly parallel to the surface. If this combined pad is detached by keeping H_1 fixed and maintaining a tilt of 1° with the surface (path 2), the forces dramatically reduces, with around 10 times reduction in the adhesion compared to path 1. We can also detach the pad by switching between the different mechanisms. Path 3 shows one such example, where, initially the leg is pulled vertically up while keeping H_1 fixed, stretching the hairs similar to path 1. On reaching point a, H_1 is set free, which results in a sudden drop in force due to the excess moment by the stretched hairs, tilting the array. Beyond this, the force curve follows the *free pull* mechanism, with ∼3.5 times reduction in adhesion. An alternate strategy of switching between mechanisms would be to first apply a load on the pad (path 4) and compress the hairs until point b. Beyond this point, the claw can be used as a hinge to detach the pad via flexing it around H_3, which once again reduces the adhesion force. Now, if we assume the joint H_2 to be free such that the two pads can behave distinctly, we can consider the scenario where the proximal pad is flexed around the distal pad at H_2 while keeping H_1 fixed (path 5). After the proximal pad has completely detached, H_1 can be freed up at point c to detach the distal pad via *free pull* with very little force. This pathway results in a ∼5 times reduction in adhesion.

The above analysis illustrates how the design of the beetle's hairy adhesive pads is suitable for modulating its adhesion. Effective control

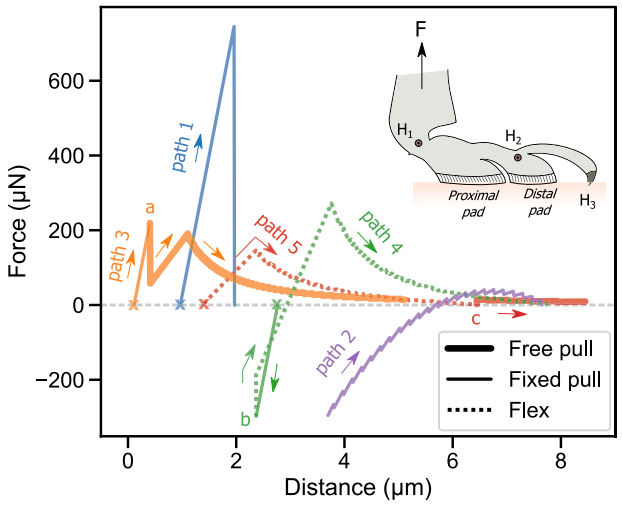

Fig. 7. Beetle leg detachment pathways. Force curves showing the theoretical detachment pathways possible for a dock beetle's leg, as function of distance between the pad and the surface. The curves are offset laterally for clarity. Colours represent the distinct detachment pathways, labelled as path 1 to 5, with arrows indicating the direction of retraction. Points a, b and c indicate instances of switching between the different detachment mechanisms for paths 3, 4 and 5 respectively (see text for details). The different line style denotes the specific detachment mechanism followed by any region of the pathway. The inset schematic shows the assumed locations of the different joints or hinges (H_1, H_2 and H_3) employed by the leg.

and release of its joints can help the insect to reduce the pad's adhesion, allowing it to detach with little effort. High reduction in adhesion is seen when the pad is tilted relative to the surface during detachment, as a result of *elastic weakening*. To the best of our knowledge, there is no direct experimental evidence that beetles or any other animal can modulate its adhesion by taking advantage of this effect. Considering that hair deformation occurs at length scales below 10 μm, direct observation of this effect on running beetles would be challenging. A recent study on PDMS micro-pillar arrays, however, does indeed show a strong reduction in the adhesion force due to slight misalignments with the surface (Booth et al., 2018). Based on previously reported microscopic investigation of freely walking dock beetles (Gernay et al., 2017), we argue that the following experimental observations provide support to our proposed model: (1) The detachment was shown to follow a three-dimensional twist of the leg, which suggests a complex inhomogeneous deformation of hairs across the array, leading to *elastic weakening*, which is suited for easy detachment. Similar twisting action during detachment was also observed in flies (Niederegger and Gorb, 2003) and has been used to easily detach mushroom-shaped artificial adhesive arrays (Kang et al., 2017). (2) The beetle can at times instantaneously detach all its legs and drop itself while upside down. This could be explained by the beetle freeing up its joints and using just its body weight to provide the necessary force to detach all its legs via *free pull* (similar to path 3 above). Lateral video recordings showed that in this scenario, claws were the last to detach when a leg loses contact with the surface, which also indicates a *flex* mode of detachment (similar to path 5). (3) Only a fraction of the beetle's pads made contact with the surface during locomotion, which indicates that the pads should naturally be in a slightly tilted state. This not only reduces the contact area, but also non-uniformly deforms the hairs, both leading to a reduction in adhesion for easy detachment. (4) Contact images showed that the array *peels* from the proximal to distal direction during detachment. However, the beetle's hairs are attached to a relatively stiff backing (Peisker et al., 2013), so it would not be able to *peel* its array, since peeling, strictly speaking, depends on the elastic contribution of a thin flexible backing as it bends during the process (Kendall, 1975). Rather, the *peeling* observed in the beetle's case should be a result of the pad detaching from the surface in a tilted orientation, causing the hairs to distinctly detach in sequence. (5) The time scale of detachment was reported to be an order of magnitude shorter than the attachment time scale, which could be a result of the elastic recoil of the leg causing a spontaneous propagation of the detachment front (Fig. 2).

There exists a limit to how much the pad can tilt, depending on its geometry and material properties. Suppose the hair has a maximum linear elastic strain limit, ϵ_m, and natural length, $l_{h,0}$. Based on Fig. 1, if the right most hair is compressed to its elastic limit, one can derive from simple geometry, that, the corresponding maximum limit in tilt angle is given by:

$$\theta_{limit} = \arctan \frac{l_{h,0}\epsilon_m}{(N_l - 1)\, w}$$

θ_{limit} will limit the reduction factor for each of the detachment mechanisms presented. Longer hairs can result in a lateral collapse or bundling of hairs, imposing an additional constraint on θ_{limit}. Large deformation of hairs can also lead to buckling, which will further limit the reduction in adhesion due to the smaller effective modulus. Buckling could also, interestingly, promote easier detachment in the *free pull* mode. When the compressed hairs at one end of the array buckle, there would be an excess clockwise moment in the array system (Fig. 3). This excess moment could subsequently drive the detachment of the remaining hairs. In the case of biological systems, the ability of an insect to provide the load necessary to tilt and compress its hairy adhesive pad against the surface would further introduce limitations to follow any of the detachment modes discussed here. All things considered, the geometry and elastic properties of the individual hairs are crucial parameters to consider in the design of an optimal array system which shows reversible adhesion via *elastic weakening*.

Our analysis had been limited to normal forces during detachment. A similar analysis considering the energy required to detach the array will however not yield any *elastic weakening* effect. Since we had assumed a purely elastic system, the initial and final energy of the system would be the same regardless of the mode of detachment, and thus the work of adhesion would remain identical in all scenarios. The reduction of adhesion force is however advantageous since an insect would not then need a strong muscular to system to detach its legs, which are typically capable of attachment forces several times its body weight (Endlein and Federle, 2007).

5. Conclusion

Controlled detachment of a fibrillar system similar to an insect's tarsal hairy adhesive pads can be achieved by either (1) pulling the pad while maintaining a constant tilt angle, (2) pulling the pad while maintaining a free tibia-tarsus leg joint or (3) flexing the pad around the claw. In all three scenarios, an inhomogeneous deformation of hairs across the array results in significant reductions in the net adhesion due to an elastic effect. Strategic control of the joint's mobility or claw can allow the leg to easily switch between the above mechanisms, thus providing a simple way to reduce adhesion as per necessity. The presence of a deformable leg can further trigger a spontaneous propagation of hair detachment due to the leg's elastic recoil, making it suitable for fast detachment. Arrays with low $\hat{f}_p$ and large number of hairs, with a hair geometry that allows for large deformations while avoiding buckling and lateral bundling represent the optimal design conditions to maximize the range of control over adhesion. The proposed model has been compared with previously reported experimental observations of leg detachment in dock beetles and highlights possible role of the joint and claws to enable reversible adhesion. Similar strategies could potentially be adopted in the design of bio-inspired artificial fibrillar adhesives to easily switch the adhesion state without the need of asymmetric structures.

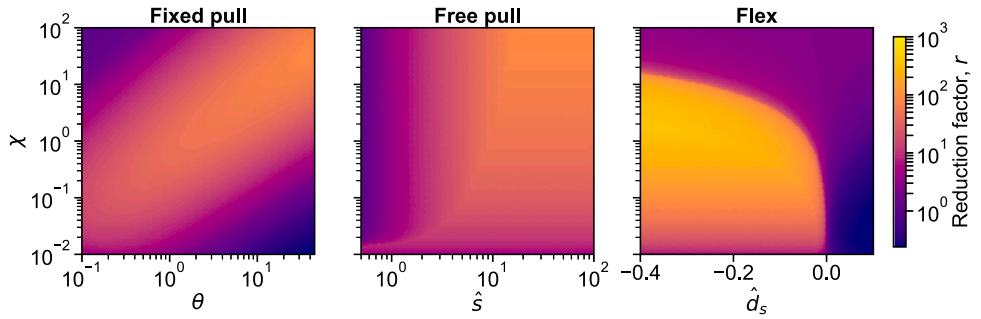

Fig. A.1. Effect of χ on reduction factor. Here, we define a unified dimensionless design parameter $\chi = \frac{f_p N_t}{k_h w}$, combining f_p and N_t into a single number. The dimensionless parameters $\hat{d}_s = \frac{d_s - l_{h,0}}{w}$ and $\hat{s} = \frac{s}{L}$, as described in text.

CRediT authorship contribution statement

Pranav Sudersan: Conceptualization, Methodology, Investigation, Software, Writing – original draft, Reviewing and editing. **Michael Kappl:** Supervision, Conceptualization, Validation, Writing – review & editing.

Declaration of competing interest

The authors declare that they have no known competing financial interests or personal relationships that could have appeared to influence the work reported in this paper.

Acknowledgements

We are grateful to Prof. Dr. Hans-Jürgen Butt and Dr. Thomas Endlein (Max Planck Institute for Polymer Research, Germany) for reviewing the text, and thank Dr. Renè Hensel (Leibniz Institute for New Materials, Germany) and Dr. Bat-El Pinchasik (Tel-Aviv University, Israel) for fruitful discussions. This work was supported by the Deutsche Forschungsgemeinschaft, Germany [Grant number: PI 1351/2-1] and the Max Planck Graduate Center, Germany with the Johannes Gutenberg-Universität Mainz [MPGC].

Appendix A. Reduction factor: master plot

See Fig. A.1.

Appendix B. Derivations

Suppose at a particular instant (Fig. 1), there are n hairs in contact with the surface. The centre of the region of the array in contact is at a vertical distance, d', from the surface. The net force on the whole array is,

$$F_{net} = \sum_{i=1}^{n} k_h \left(l_{h,i} - l_{h,0}\right)$$

$l_{h,i}$ is the length of the ith hair, which is at a horizontal distance, x_i, from the centre of the contact region. By simple geometry, $l_{h,i} = d' - x_i \tan\theta$. Substituting $l_{h,i}$ in above and noting that $\sum_{i=1}^{n} x_i = 0$ by symmetry, we get:

$$F_{net} = nk_h \left(d' - l_{h,0}\right)$$

From geometry, d_s and d' is related as:

$$\frac{d_s}{\sin\theta} - \frac{d'}{\sin\theta} = s - \frac{(n-1)\,w}{2}$$

Substituting for d', the net force, F_{net}, on the pad as a function of distance, d_s, is:

$$F_{net} = nk_h \left[d_s - l_{h,0} - \left[s - \frac{(n-1)\,w}{2}\right]\sin\theta\right]$$

The above equation is valid for $d_s \le d_{s,max}$ at a particular value of n. We can get $d_{s,max}$ by considering the situation just before the left most hair is about to detach (Fig. 1). This hair will be at its maximum length, $l_{h,p}$. Once again from geometry, we see that $d_{s,max}$ and $l_{h,p}$ is related as:

$$\frac{l_{h,p}}{\sin\theta} - \frac{d_{s,max}}{\sin\theta} = (n-1)\,w - s$$

Substituting $l_{h,p} = \frac{f_p}{k_h} + l_{h,0}$ in above and simplifying, we get:

$$d_{s,max} = l_{h,0} + \frac{f_p}{k_h} + [s - (n-1)\,w]\sin\theta$$

The net moment about the joint due to the deformed hairs of the array is,

$$M_{net} = \sum_{i=1}^{n} \lambda_i k_h \left(l_{h,i} - l_{h,0}\right)\cos\theta$$

Here, $\lambda_i = s - \left(\frac{n-1}{2}w - \frac{x_i}{\cos\theta}\right)$ is the length of the lever arm between the ith hair and the joint.

Substituting for $l_{h,i}$ and eliminating d' as before, we get:

$$M_{net} = \sum_{i=1}^{n} k_h \cos\theta \left[s - \left(\frac{n-1}{2}w - \frac{x_i}{\cos\theta}\right)\right] \times \left[d_s - \left(s - \frac{(n-1)\,w}{2}\right)\sin\theta - x_i\tan\theta - l_{h,0}\right]$$

To calculate $\sum_{i=1}^{n} x_i^2$, we follow:

$$\sum_{i=1}^{n} x_i^2 = 2\sum_{i=1}^{\frac{n}{2}} x_i^2 = 2\sum_{i=1}^{\frac{n}{2}} \left[w\cos\theta\left(i - \frac{1}{2}\right)^2\right] = 2w^2\cos^2\theta\left[\sum_{i=1}^{\frac{n}{2}} i^2 - \sum_{i=1}^{\frac{n}{2}} i - \sum_{i=1}^{\frac{n}{2}} \frac{1}{4}\right]$$

Using the identities $\sum_{i=1}^{N} i^2 = \frac{N(N+1)}{2}$ and $\sum_{i=1}^{N} i^2 = \frac{N(N+1)(2N+1)}{6}$ and simplifying, we get $\sum_{i=1}^{n} x_i^2 = n\left(\frac{n^2-1}{12}\right)w^2\cos^2\theta$. This, together with $\sum_{i=1}^{n} x_i = 0$ (by symmetry), the expression for M_{net} above can be simplified to finally get:

$$M_{net} = nk_h\cos\theta\left[\left(d_s - l_{h,0}\right)\left[s - \frac{(n-1)\,w}{2}\right] - \left\{\left[s - \frac{(n-1)\,w}{2}\right]^2 + \frac{n^2-1}{12}w^2\right\}\sin\theta\right]$$

References

Autumn, K., Liang, Y.A., Hsieh, S.T., Zesch, W., Chan, W.P., Kenny, T.W., Fearing, R., Full, R.J., 2000. Adhesive force of a single gecko foot-hair. Nature 405 (6787), 681–685. http://dx.doi.org/10.1038/35015073.

Bacca, M., Booth, J.A., Turner, K.L., McMeeking, R.M., 2016. Load sharing in bioinspired fibrillar adhesives with backing layer interactions and interfacial misalignment. J. Mech. Phys. Solids 96, 428–444. http://dx.doi.org/10.1016/j.jmps.2016.04.008.

Booth, J.A., Bacca, M., McMeeking, R.M., Foster, K.L., 2018. Benefit of backing-layer compliance in fibrillar adhesive patches-resistance to peel propagation in the presence of interfacial misalignment. Adv. Mater. Interfaces 5 (15), 1800272. http://dx.doi.org/10.1002/admi.201800272.

Bullock, J.M., Federle, W., 2009. Division of labour and sex differences between fibrillar, tarsal adhesive pads in beetles: effective elastic modulus and attachment performance. J. Exp. Biol. 212 (Pt 12), 1876–1888. http://dx.doi.org/10.1242/jeb.030551.

Bullock, J.M., Federle, W., 2011. Beetle adhesive hairs differ in stiffness and stickiness: in vivo adhesion measurements on individual setae. Naturwissenschaften 98 (5), 381–387. http://dx.doi.org/10.1007/s00114-011-0781-4.

del Campo, A., Greiner, C., Arzt, E., 2007. Contact shape controls adhesion of bioinspired fibrillar surfaces. Langmuir 23 (20), 10235–10243. http://dx.doi.org/10.1021/la7010502.

Carbone, G., Pierro, E., Gorb, S.N., 2011. Origin of the superior adhesive performance of mushroom-shaped microstructured surfaces. Soft Matter 7 (12), 5545–5552. http://dx.doi.org/10.1039/C0SM01482F.

Chary, S., Tamelier, J., Turner, K., 2013. A microfabricated gecko-inspired controllable and reusable dry adhesive. Smart Mater. Struct. 22 (2), 025013. http://dx.doi.org/10.1088/0964-1726/22/2/025013.

Cui, J., Drotlef, D.-M., Larraza, I., Fernández-Blázquez, J.P., Boesel, L.F., Ohm, C., Mezger, M., Zentel, R., del Campo, A., 2012. Bioinspired actuated adhesive patterns of liquid crystalline elastomers. Adv. Mater. 24 (34), 4601–4604. http://dx.doi.org/10.1002/adma.201200895.

Drotlef, D.-M., Blümler, P., del Campo, A., 2014. Magnetically actuated patterns for bioinspired reversible adhesion (dry and wet). Adv. Mater. 26 (5), 775–779. http://dx.doi.org/10.1002/adma.201303087.

Endlein, T., Federle, W., 2007. To stick and not getting stuck — detachment control in ants. Comp. Biochem. Physiol. A: Mol. Integr. Physiol.. 146 (4, Supplement), S121–S122. http://dx.doi.org/10.1016/j.cbpa.2007.01.222, Abstracts of the Annual Main Meeting of the Society for Experimental Biology, Glasgow, Scotland, 31st March - 4th April, 2007.

Endlein, T., Ji, A., Samuel, D., Yao, N., Wang, Z., Barnes, W.J.P., Federle, W., Kappl, M., Dai, Z., 2013. Sticking like sticky tape: tree frogs use friction forces to enhance attachment on overhanging surfaces. J. R. Soc. Interface 10 (80), 20120838. http://dx.doi.org/10.1098/rsif.2012.0838.

Federle, W., 2006. Why are so many adhesive pads hairy? J. Exp. Biol. 209 (Pt 14), 2611–2621. http://dx.doi.org/10.1242/jeb.02323.

Gernay, S.M., Labousse, S., Lambert, P., Compere, P., Gilet, T., 2017. Multi-scale tarsal adhesion kinematics of freely-walking dock beetles. J. R. Soc. Interface 14 (136), 20170493. http://dx.doi.org/10.1098/rsif.2017.0493.

Gouravaraju, S., Sauer, R.A., Gautam, S.S., 2021. On the presence of a critical detachment angle in gecko spatula peeling - a numerical investigation using an adhesive friction model. J. Adhes. 97 (13), 1234–1254. http://dx.doi.org/10.1080/00218464.2020.1746652.

Grill, M.J., Meier, C., Wall, W.A., 2021. Investigation of the peeling and pull-off behavior of adhesive elastic fibers via a novel computational beam interaction model. J. Adhes. 97 (8), 730–759. http://dx.doi.org/10.1080/00218464.2019.1699795.

Heepe, L., Carbone, G., Pierro, E., Kovalev, A.E., Gorb, S.N., 2014. Adhesion tilt-tolerance in bio-inspired mushroom-shaped adhesive microstructure. Appl. Phys. Lett. 104 (1), 011906. http://dx.doi.org/10.1063/1.4860991.

Hensel, R., Thiemecke, J., Booth, J.A., 2021. Preventing catastrophic failure of microfibrillar adhesives in compliant systems based on statistical analysis of adhesive strength. ACS Appl. Mater. Interfaces 13 (16), 19422–19429. http://dx.doi.org/10.1021/acsami.1c00978.

Hooke, R., 1665. Micrographia, or, Some Physiological Descriptions of Minute Bodies Made by Magnifying Glasses : with Observations and Inquiries Thereupon. The Royal Society, London.

Hui, C.Y., Glassmaker, N.J., Tang, T., Jagota, A., 2004. Design of biomimetic fibrillar interfaces: 2. Mechanics of enhanced adhesion. J. R. Soc. Interface 1 (1), 35–48. http://dx.doi.org/10.1098/rsif.2004.0005.

Jagota, A., Stephen, J.B., 2002. Mechanics of adhesion through a fibrillar microstructure. Integr. Comp. Biol. 42 (6), 1140–1145.

Kamperman, M., Kroner, E., del Campo, A., McMeeking, R.M., Arzt, E., 2010. Functional adhesive surfaces with "Gecko" effect: The concept of contact splitting. Adv. Energy Mater. 12 (5), 335–348. http://dx.doi.org/10.1002/adem.201000104.

Kang, O.H., Lee, S.H., Yun, J.H., Yi, H., Kwak, M.K., Lee, S.R., 2017. Adhesion tunable bio-inspired dry adhesives by twisting. Int. J. Precis. Eng. Manuf. 18 (10), 1433–1437. http://dx.doi.org/10.1007/s12541-017-0171-8.

Kendall, K., 1975. Thin-film peeling-the elastic term. J. Phys. D: Appl. Phys. 8 (13), 1449–1452. http://dx.doi.org/10.1088/0022-3727/8/13/005.

Kim, J.-K., Varenberg, M., 2017. Biomimetic wall-shaped adhesive microstructure for shear-induced attachment: the effects of pulling angle and preliminary displacement. J. R. Soc. Interface 14 (137), 20170832. http://dx.doi.org/10.1098/rsif.2017.0832.

Kizilkan, E., Strueben, J., Staubitz, A., Gorb, S.N., 2017. Bioinspired photocontrollable microstructured transport device. Sci. Robot. 2 (2), eaak9454. http://dx.doi.org/10.1126/scirobotics.aak9454.

Kligerman, Y., Breitman, P., Varenberg, M., 2020. Biomimetic wall-shaped hierarchical micro-structure: Numerical simulation of sliding inception. Bioinspiration Biomim. 15 (4), 046011. http://dx.doi.org/10.1088/1748-3190/ab8ba3.

Labonte, D., Federle, W., 2015. Scaling and biomechanics of surface attachment in climbing animals. Philos. Trans. R. Soc. Lond. B Biol. Sci. 370 (1661), 20140027. http://dx.doi.org/10.1098/rstb.2014.0027.

Langer, M.G., Ruppersberg, J.P., Gorb, S., 2004. Adhesion forces measured at the level of a terminal plate of the fly's seta. Proc. R. Soc. B 271 (1554), 2209–2215. http://dx.doi.org/10.1098/rspb.2004.2850.

Mengüç, Y., Yang, S.Y., Kim, S., Rogers, J.A., Sitti, M., 2012. Gecko-inspired controllable adhesive structures applied to micromanipulation. Adv. Funct. Mater. 22 (6), 1246–1254. http://dx.doi.org/10.1002/adfm.201101783.

Murphy, M.P., Aksak, B., Sitti, M., 2007. Adhesion and anisotropic friction enhancements of angled heterogeneous micro-fiber arrays with spherical and spatula tips. J. Adhes. Sci. Technol. 21 (12–13), 1281–1296. http://dx.doi.org/10.1163/156856107782328380.

Niederegger, S., Gorb, S., 2003. Tarsal movements in flies during leg attachment and detachment on a smooth substrate. J. Insect Physiol. 49 (6), 611–620. http://dx.doi.org/10.1016/s0022-1910(03)00048-9.

O'Rorke, R.D., Steele, T.W.J., Taylor, H.K., 2016. Bioinspired fibrillar adhesives: a review of analytical models and experimental evidence for adhesion enhancement by surface patterns. J. Adhes. Sci. Technol. 30 (4), 362–391. http://dx.doi.org/10.1080/01694243.2015.1101183.

Pantano, A., Pugno, N.M., Gorb, S.N., 2011. Numerical simulations demonstrate that the double tapering of the spatualae of lizards and insects maximize both detachment resistance and stability. Int. J. Fract. 171 (2), 169–175. http://dx.doi.org/10.1007/s10704-011-9596-8.

Paretkar, D., Kamperman, M., Martina, D., Zhao, J., Creton, C., Lindner, A., Jagota, A., McMeeking, R., Arzt, E., 2013. Preload-responsive adhesion: effects of aspect ratio, tip shape and alignment. J. R. Soc. Interface 10 (83), 20130171. http://dx.doi.org/10.1098/rsif.2013.0171.

Peisker, H., Michels, J., Gorb, S.N., 2013. Evidence for a material gradient in the adhesive tarsal setae of the ladybird beetle *Coccinella septempunctata*. Nature Commun. 4, 1661. http://dx.doi.org/10.1038/ncomms2576.

Persson, B.N.J., 2003. On the mechanism of adhesion in biological systems. J. Chem. Phys. 118 (16), http://dx.doi.org/10.1063/1.1562192.

Popov, V.L., Filippov, A.É., Gorb, S.N., 2016. Biological microstructures with high adhesion and friction. Numerical approach. Phys.-Usp. 59, 829–845.

Sauer, R.A., Holl, M., 2013. A detailed 3D finite element analysis of the peeling behaviour of a gecko spatula. Comput. Methods Biomech. Biomed. Eng. 16 (6), 577–591. http://dx.doi.org/10.1080/10255842.2011.628944.

Schargott, M., Popov, V.L., Gorb, S., 2006. Spring model of biological attachment pads. J. Theoret. Biol. 243 (1), 48–53. http://dx.doi.org/10.1016/j.jtbi.2006.05.023.

Stork, N.E., 1980. Experimental analysis of adhesion of *Chrysolina Polita* (Chrysomelidae: Coleoptera) on a variety of surfaces. J. Exp. Biol. 88 (1), 91.

Tian, Y., Pesika, N., Zeng, H., Rosenberg, K., Zhao, B., McGuiggan, P., Autumn, K., Israelachvili, J., 2006. Adhesion and friction in gecko toe attachment and detachment. Proc. Natl. Acad. Sci. U.S.A 103 (51), 19320–19325. http://dx.doi.org/10.1073/pnas.0608841103.

Varenberg, M., Pugno, N.M., Gorb, S.N., 2010. Spatulate structures in biological fibrillar adhesion. Soft Matter 6, 3269–3272. http://dx.doi.org/10.1039/C003207G.

Wu, X., Wang, X., Mei, T., Sun, S., 2015. Mechanical analyses on the digital behaviour of the Tokay gecko (*Gekko gecko*) based on a multi-level directional adhesion model. Proc. R. Soc. Lond. Ser. A Math. Phys. Eng. Sci. 471 (2179), 20150085. http://dx.doi.org/10.1098/rspa.2015.0085.